THE JOURNAL OF BIOLOGICAL CHEMISTRY VOL. 284, NO. 49, pp. 34084–34091, December 4, 2009

Structural Characterization of Mouse Neutrophil Serine Proteases and Identification of Their Substrate Specificities

*RELEVANCE TO MOUSE MODELS OF HUMAN INFLAMMATORY DISEASES**

Received for publication, July 10, 2009, and in revised form, October 13, 2009 Published, JBC Papers in Press, October 15, 2009, DOI 10.1074/jbc.M109.042903

Timofey Kalupov[‡], Michèle Brillard-Bourdet[‡], Sébastien Dadé[‡], Hélène Serrano[‡], Julien Wartelle[§], Nicolas Guyot[§], Luiz Juliano[¶], Thierry Moreau[‡], Azzaq Belaaouaj[§1], and Francis Gauthier[§2]

From [‡]INSERM U618, Protéases et Vectorisation Pulmonaires, IFR 135, Université François Rabelais de Tours, 37032 Tours, France, the [¶]Departamento de Biofísica, Escola Paulista de Medicina, Universidade Federal, 04044-20 São Paulo, Brazil, and [§]INSERM AVENIR/EA 4303, Inflammation et Immunité de l'Epithélium Respiratoire, URCA, IFR 53, Hopital Maison Blanche, CHU de Reims, Reims 51092 Cedex, France

It is widely accepted that neutrophil serine proteases (NSPs) play a critical role in neutrophil-associated lung inflammatory and tissue-destructive diseases. To investigate NSP pathogenic role(s), various mouse experimental models have been developed that mimic acutely or chronically injured human lungs. We and others are using mouse exposure to cigarette smoke as a model for chronic obstructive pulmonary disease with or without exacerbation. However, the relative contribution of NSPs to lung disease processes as well as their underlying mechanisms remains still poorly understood. And the lack of purified mouse NSPs and their specific substrates have hampered advances in these studies. In this work, we compared mouse and human NSPs and generated three-dimensional models of murine NSPs based on three-dimensional structures of their human homologs. Analyses of these models provided compelling evidence that peptide substrate specificities of human and mouse NSPs are different despite their conserved cleft and close structural resemblance. These studies allowed us to synthesize for the first time novel sensitive fluorescence resonance energy transfer substrates for individual mouse NSPs. Our findings and the newly identified substrates should better our understanding about the role of NSPs in the pathogenesis of cigarette-associated chronic obstructive pulmonary disease as well as other neutrophils-associated inflammatory diseases.

Neutrophil serine proteases (NSPs),[3] neutrophil elastase (NE), cathepsin G (CG), and proteinase 3 (Pr3), are mainly stored in neutrophil primary granules in readily active forms. NSPs are structurally related and share the conserved charge-relay triad, His^{57}–Asp^{102}–Ser^{195}, where Ser is the active residue (chymotrypsinogen numbering) (1). NSPs contribute to neutrophil oxygen-independent system-mediated protection of the host against invading pathogens (2). Indeed, NSPs serve a physiological role for killing of microbes (3). Activated neutrophils are also known to release NSPs in the setting of inflammation. *In vitro*, NSPs are capable of cleaving a panoply of substrates. These include extracellular matrix proteins, pro-inflammatory mediators, coagulation factors, and immunoglobulins (4). NE degrades pro-inflammatory mediators such as tumor necrosis factor-α and interleukin-1β, hence could alter the inflammatory response. The enzyme is capable of inducing the secretion of granulocyte macrophage-colony stimulating factor and interleukin-8, which could amplify the inflammation. Consequently, the release of these potent proteinases in diseased situations could create a proteolytic environment where degradation of different host molecules might occur and result in inappropriate inflammatory response. Because of their large substrate repertoire, NSPs have been implicated in the pathogenesis of various inflammatory and tissue-destructive diseases, including acute lung injury, cystic fibrosis, and COPD (5–7).

COPD is recognized as a major health problem whose worldwide incidence is increasing dramatically. Cigarette smoke represents the major etiologic factor contributing to the development and progression of COPD. Advances in therapy against COPD have been limited due in part to poor understanding of the pathogenesis of this disease. Various animal models and injurious stimuli mimicking human COPD are now available to help understand the development of this pathology (reviewed in Ref. 8). For example, several inbred strains of mice spontaneously develop emphysema, the main component of COPD, due to genetic abnormalities (reviewed in Ref. 8). And mice exposed to cigarette smoke provide a valuable model of human COPD (9).

The contribution of NSPs to COPD was first evidenced by the observation that patients lacking α1-Pi, the main physiological inhibitor of neutrophil elastase, were at greater risk of developing emphysema (10, 11). Subsequently, various studies reported the induction of emphysema in animal models following instillation of NSPs. Intratracheal instillation of mice with human neutrophil elastase or proteinase 3 leads to tissue

* This work was supported by the Agence Nationale de la Recherche (ANR), Contract ANR-07-PHYSIO-029-01.

[1] To whom correspondence may be addressed: INSERM AVENIR/EA4303, 45, Cognacq Jay St., Reims 51092 Cedex, France. Tel.: 33-3-26-78-39-06; Fax: 33-3-26-06-58-61; E-mail: azzaq.belaaouaj@univ-reims.fr.

[2] To whom correspondence may be addressed: Faculty of Medicine, 10 Bd. Tonnellé, 37032 Tours, France. Tel.: 33-2-47-366045; Fax: 33-2-47-366046; E-mail: francis.gauthier@univ-tours.fr.

[3] The abbreviations used are: NSP, neutrophil serine protease; COPD, chronic obstructive pulmonary disease; hNE, human neutrophil elastase; hPr3, human proteinase 3; hCG, human cathepsin G; mNE, mouse neutrophil elastase; mPr3, mouse proteinase 3; mCG, mouse cathepsin G; α1-Pi, α 1-protease inhibitor; ACT, antichymotrypsin; FRET, fluorescence resonance energy transfer; HPLC, high-performance liquid chromatography.

destruction and airspace enlargement, characteristic features of emphysema (12). In recent years, it has been shown that mice deficient in NE are considerably protected against cigarette-induced emphysema. Despite these compelling observations, the mechanisms by which NSPs injure the lung are not understood. Part of this concern may be because full characterization of mouse NSPs is still lacking. Although we and others have cloned and characterized murine NSPs genes/cDNAs (13–15), their corresponding proteins have not been purified. More importantly, unlike human NSPs, no specific peptides substrates for mouse NSPs are available to detect and quantify their specific activities especially in disease models.

To address these concerns, we purified the three mouse NSPs and carried out a detailed analysis by comparison to human NSPs. Our studies revealed critical differences between mouse and human NSPs, which prompted us to develop new specific FRET peptides substrates for mouse NSPs. Molecular modeling approach in association with kinetic studies enabled us to generate/synthesize new sensitive substrates to both detect and measure all three mouse NSPs activities in the subnanomolar range.

EXPERIMENTAL PROCEDURES

Reagents—Human neutrophil elastase (hNE, EC 3.4.21.37), cathepsin G (hCG, EC 3.4.21.20), α1-antichymotrypsin, and α1-protease inhibitor (α1-Pi) were obtained from Biocentrum Ltd. (Krakow, Poland), and Proteinase 3 (hPr3, EC 3.4.21.76) was from Athens Research and Technology (Athens, GA). All other chemicals were reagent grade and purchased from Sigma-Aldrich, unless otherwise stated.

Mice and Neutrophils—Wild-type mice (n = 15) had C57/BL6 genetic background and were 8–10 weeks old. Mice were maintained in the animal barrier facility with a 12-h light/dark cycle and provided with water and food *ad libitum*. All procedures were approved by the Animal Studies Committee of our institute.

Mouse neutrophils were isolated from peritoneal lavage fluids after they were attracted to the peritoneum by intraperitoneal injection of 15% glycogen (1 ml/mouse) (16). At 16 h post-challenge, mice were sacrificed by cervical dislocation. The peritoneal cavities were lavaged with 5 ml of phosphate-buffered saline, and the lavage fluids were spun and resuspended in a hypotonic lysis solution to remove red cell contamination. Next, the number and viability of cells in the lavage fluid were determined by hemacytometer and trypan blue exclusion, respectively. For differential counts, cells were cytospun (Cytospin 4, Thermo Shandon, Pittsburgh, PA) and stained with a modified Wrights stain (Hema 3, Fisher Scientific, Middletown, VA). The cell pellet was resuspended in phosphate-buffered saline supplemented with 0.15% Brij 35.

Purification of Murine Neutrophil Serine Proteases—Cell pellet was subjected to three cycles of freezing and thawing. Following the first cycle, the cell suspension was sonicated for 3 × 1-min with 2 × 1-min intervals on ice. The cell suspension was centrifuged after each cycle, and supernatants were collected and diluted in two volumes of 50 mM phosphate-buffered saline, pH 7.4, to adjust the Brij concentration to 0.05%. Pooled supernatants were run on a heparin-Sepharose column (10 ml) at 4 °C. Recovered fractions from the column washing step, and fractions eluted with a 0.05–0.8 M NaCl gradient (2 × 25 ml) were assayed against a polyvalent fluorogenic substrate sensitive to both trypsin-like and chymotrypsin-like proteases, Abz-HPVPVYAFSPQ-EDDnp. Fractions with peptidase activity from the column washing step and following elution with a 0.05–0.8 M NaCl gradient were pooled separately. The pool derived from the column washing fractions was loaded onto a phenyl-Sepharose column pre-equilibrated in 0.3 M sodium acetate (NaOAc), pH 5.5. Protein elution was carried out with a linear gradient (0–50%) of 2-propanol in 0.05 M NaOAc, pH 5.5. Active fractions against Abz-HPVPVYAFSPQ-EDDnp were pooled and equilibrated in 0.3 M NaOAc, pH 5.5, 25% 2-propanol and stored at −20 °C. An aliquot was subjected to HPLC on a C4 column (2.1 mm × 30 mm) eluted (0.2 ml/min) with a linear 0–60% (v/v) gradient of acetonitrile in 0.075% trifluoroacetic acid. The N-terminal amino acid sequences of selected protein fractions were determined by automated Edman degradation as described below. The pool of active fractions recovered from the NaCl gradient was run on SP-Sepharose pre-equilibrated in 0.05 M phosphate buffer, pH 7.4, 150 mM NaCl, 0.05% Brij 35. Buffers containing 0.5 M NaCl buffer and 0.8 M NaCl were employed to elute trypsin-like protease fractions and chymotrypsin-like protease fractions, respectively. Aliquots from the pooled trypsin-like protease fractions and chymotrypsin-like protease fractions were subjected to HPLC on a C4 column. The N-terminal amino acid sequences of selected protein fractions were determined by automated Edman degradation as described below.

Immunoblotting—Prior to NSP purification, cell lysates were subjected to immunoblotting. Aliquots of protein fractions were resolved by SDS-PAGE and processed for Western blotting experiment. The membranes were sequentially incubated with rabbit polyclonal antibody specific to individual mouse NSPs (NE (1:2,000), PR 3 (1:2,000), and CG (1:500)) followed by goat anti-rabbit horseradish peroxidase (17). Immunoreactive fragments were visualized by enhanced chemiluminescence as previously described.

N-terminal Sequencing—N-terminal amino acid sequencing of selected peak were determined using an Applied Biosystems Procise 494 sequencer attached to a Model 140C Micro-gradient System and a 610A Data Analysis System with the chemicals and program recommended by the manufacturer (Applied Biosystems, Courtaboeuf, France).

Synthesis of FRET Peptide Substrates—FRET fluorogenic Abz-peptidyl-EDDnp substrates for human and mouse neutrophil serine proteases were synthesized as previously reported (18). Substrates were purified by semipreparative reversed-phase chromatography using a 50-min linear (0–100%) gradient of acetonitrile in 0.1% trifluoroacetic acid and checked for homogeneity by analytic reversed-phase HPLC on a C18 column and matrix-assisted laser desorption ionization time-of-flight mass spectrometry (TofSpec-E, Micromass, Manchester, UK) or peptide sequencing. Stock substrate solutions (2–5 mM) were prepared in 30% (v/v) *N,N′*-dimethylformamide and diluted to 0.5 mM with 50 mM Hepes buffer, pH 7.4. Stock solutions of Cys-containing substrates were supplemented with 10 mM dithiothreitol.

Enzyme Assays—Protease activities were assayed in 50 mM Hepes, pH 7.4, 150 mM NaCl, supplemented with 0.05% Igepal CA-630 (v/v) to prevent protease sticking to plastic and glass surfaces. Purified mouse NE (mNE) and mouse Pr3 (mPr3) were titrated with human α1-PI and mouse CG (mCG) with human ACT (19, 20).

The activities of mNE, mPr3, and mCG were first examined using the polyvalent FRET substrate Abz-HPVPVYAFSPQ-EDDnp. Substrate hydrolysis was followed by measuring the fluorescence at ex = 320 nm and em = 420 nm, as reported earlier (18, 21).

Specificity constants (k_{cat}/K_m) were determined under first-order conditions using substrate concentrations far below the K_m (maximum, 1 μM). The final concentration of all three enzymes was in the nanomolar range. The sites in the FRET substrates cleaved by mouse and human proteases were identified by mass spectrometry and/or N-terminal sequencing. Fluorogenic substrates (5–8 μM final) were incubated with human or mouse Pr3, NE, and CG (1–10 nM) in reaction buffer at 37 °C. The reaction was stopped by adding 4 volumes of absolute ethanol and incubating for 15 min on ice. Precipitated protein was removed by centrifugation at 13,000 × *g* for 10 min. The supernatant containing the hydrolysis products was dried under vacuum and dissolved in 200 μl of 0.01% trifluoroacetic acid (v/v). Hydrolysis fragments were purified by reversed-phase chromatography on a C18 column (2.1 mm × 30 mm) eluted at 0.3 ml/min with a linear (0–60%, v/v) gradient of acetonitrile in 0.01% trifluoroacetic acid for 20 min. Eluted peaks were monitored at three wavelengths (220, 320, and 360 nm) simultaneously to directly identify EDDnp-containing peptides prior to sequencing.

Modeling of Murine Neutrophil Serine Proteases—Because human and mouse NSPs share ~70% sequence identity, we used various automated comparative modeling tools to generate models of murine NSPs based on the three-dimensional structure templates of HNE, hPr3, and hCG, respectively. These include Swiss-Model, $(PS)^2$, and ModWeb. The sequences of mNE (UniProtKB entry name ELNE_MOUSE), mPr3 (UniProtKB entry name PRTN3_MOUSE), and mCG (UniProtKB entry name CATG_MOUSE) were used as inputs for the automatic modeling mode. All the models were then evaluated using ANAOLEA to analyze the non-local environment of each heavy atom in the protein structure and EVAL123D, which allows evaluation of three-dimensional protein structures by different methods (Verify3D, Eval23D, ProsaII, EvTree, and SFE) in a single run. Based on this analysis, we found that Swiss-Model provides the best models for murine NSPs. All subsequent studies were carried based on these models.

Electrostatic Potential Calculations—The electrostatic potentials of mNE, mPr3, and mCG were calculated using the finite difference Poisson Boltzmann method as implemented in DELPHI software (INSIGHT II suite, Accelrys Inc.). The ionic strength was set to 0.15 M, and the dielectric constant to 4 for the protein interior and 80 for the solvent. Calculations were performed at pH 7.4 at a temperature of 300 K. Formal charges, rather than all charges, were assigned as follows: arginine, lysine, N terminus, +1; glutamate, aspartate, C terminus, −1; and histidine, neutral. Contours of electrostatic potentials were displayed at ± 5 kTe^{-1} using INSIGHT II. The locations of the various subsites in the active site of each protease were inferred from the positions of the side chains of the corresponding residues of the OMT3 inhibitor complexed with HNE (PDB entry code 1PPF). The solvent-accessible molecular surface was calculated and colored according to the electrostatic potential using Insight II (Accelrys Inc.).

RESULTS AND DISCUSSION

In the present work, we purified mouse neutrophil serine proteases and characterized them by comparison to their human counterparts. This allowed us to generate sensitive peptide substrates to individual murine proteases namely mNE, mCG, and mPr3.

Purification of Mouse NE, CG, and Pr3—As shown in Fig. 1*A*, intraperitoneal instillation of glycogen resulted in massive recruitment of inflammatory cells. In accordance with our previous work and as judged by morphologic criteria, the cellular infiltrate was predominately neutrophils. Mouse peritonea were lavaged, and collected cells were processed for NSPs purification as outlined under "Experimental Procedures." To ensure the presence of mouse NSPs, aliquots of cell protein extracts were subjected to Western blotting using antibodies specific to mNE, mCG, and mPr3 (Fig. 1*B*). Next, mouse NSPs were extracted/purified as outlined in Fig. 1*C*. Following loading of neutrophil protein extracts on heparin-Sepharose column, we detected peptidase activity in both flow-through and NaCl gradient-eluted fractions using our polyvalent FRET substrate Abz-HPVPVYAFSPQ-EDDnp, a peptide sensitive to both trypsin- and chymotrypsin-like human proteases. The eluted fraction showed an asymmetric peak and was subjected to further fractionation using cation-exchange chromatography. This step allowed us to identify/separate peptidase activities into two fractions. The flow-through fraction of the heparin column was loaded onto phenyl-Sepharose, and peptidase activity was found in the fraction eluted with 50% isopropanol (Fig. 1*C*). All three fractions were HPLC-purified and processed for N-terminal amino acid sequencing. Peptide sequence analyses found that the phenyl-Sepharose fraction corresponded to mPr3, whereas each of the two fractions with peptidase activity eluted from the cation-exchange column corresponded to mNE or mCG (Fig. 1*D*). Comparison of the net charges of mouse and human NSPs showed that the murine NSPs were less cationic than their human counterparts with mCG and mPr3 being the most positively and negatively charged enzymes. Of interest, amino acid sequence analyses identified, in addition to mouse NSPs, a protein called calgranulin. This protein is a member of the EF-hand calcium-binding protein family, also known as cystic fibrosis antigen. It is expressed in neutrophils, macrophages, and epithelial cells (22). While its presence might suggest potential interaction with cationic proteases, *in vivo* significance of this finding is awaited. Interestingly, analysis of the net charge of murine NSPs calculated from their cDNA-deduced amino acid sequences support our purification strategy (Table 1). Next, the kinetic properties of all three isolated proteases were determined.

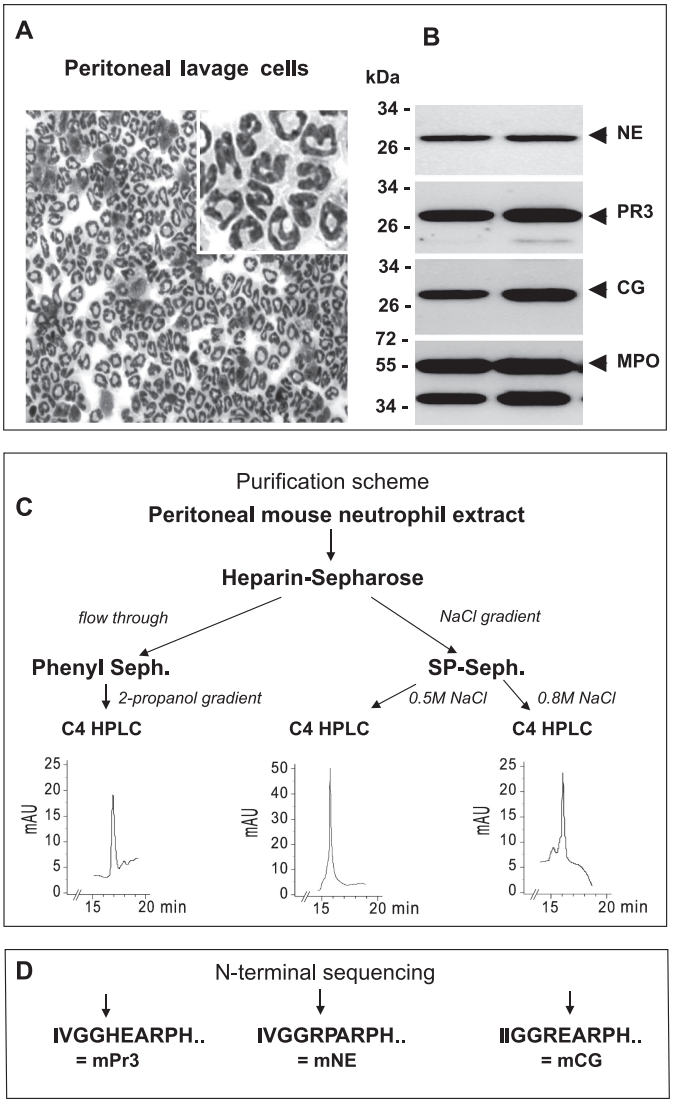

FIGURE 1. **Purification of mouse neutrophil serine proteases.** *A*, cytospins for lavage fluids at 16 h revealed that neutrophils dominated the cellular infiltrate following intraperitoneal injection of glycogen. Shown is a representative micrograph of glycogen-elicited cells (×200, *inset* ×400). *B*, immunodetection of mNE, mCG, and mPr3 in neutrophil protein extracts. *Arrowheads* indicate the position of serine proteases. Immunoblotting for MPO was used an internal control. MPO antibody detected the H chain (~59 kDa) and an autocatalytic cleavage product (~45 kDa). Molecular mass standards are shown on the *left*. *C*, scheme of purification strategy of individual mouse neutrophil serine proteases. *D*, N-terminal sequencing of the end product of protease purification resulted in an unambiguous amino acid sequence identical to mPr3, mNE, or mCG.

TABLE 1
Net charge of mouse and human neutrophil serine proteases

Net charge (pH 7.4)	Mouse	Human
Elastase	+9	+11
Proteinase 3	−2	+1
Cathepsin G	+16	+23

Characterization of Purified Mouse NSPs—In recent years, we have generated highly specific FRET substrates enabling us to detect human NSPs in the 0.1 nM range. Because of the conservation of the active site triad and the physicochemical property closeness between human and mouse NSPs, we first investigated kinetic properties of purified mNE, mCG, and mPr3 using human NSP substrates. Although incubation of hCG FRET peptide with mCG resulted in a high recorded fluorescence value, no changes in fluorescence were detected with hNE and hPr3 substrates in the presence of mNE or mPr3 (Tables 2 and 3). These data indicate that mNE and mPr3 substrate specificities differ from those of their human counterparts. In support of these differences in substrate recognition between human and mouse NSPs, the potent recombinant human elastase inhibitor EPI-hNE4 did not interact with mNE (23). However, the human serpin α1-P_i inhibited both mNE and mPr3, and human ACT inhibited mCG. In this regard, we were able to titrate the activities of the three murine proteases using Abz-HPVPVYAFSPQ-EDDnp, against mNE and mPr3, and the hCG substrate Abz-TPFSGQ-EDDnp against mCG (Fig. 2). The titrated mouse proteases were then used to raise new specific mouse NSPs substrates and to determine the kinetic parameters of their hydrolysis. To this end, we first identified the structural differences between mouse and human proteases that could potentially account for their differences in substrate specificity. We constructed molecular models of the three mouse NSPs using the three-dimensional crystal structures of their human counterparts as templates and compared the structures of the critical subsites previously identified as participating in substrate binding.

Design and Testing of Sensitive mNE Substrate—As reported in Table 2, hNE-specific FRET substrates were not cleaved by mNE. We hypothesized that the inability of mNE to target such peptides could be due to the presence of charged residues at P2–P3 and P2′–P3′.[4] In support of this hypothesis, the peptide substrate Abz-HPVPVYAFSPQ-EDDnp, which is cleaved by

TABLE 2
Specificity constants k_{cat}/K_m for the hydrolysis of FRET elastase substrates

Values are means of at least three experiments. The error for k_{cat}/K_m is <15%. Cleavage sites are indicated by a space in the peptide sequence.

	k_{cat}/K_m		
	mNE	hNE	mPr3
		$m_M^{-1}s^{-1}$	
Abz-APEEI MDRQ-EDDnp	nsh[a]	683	12
Abz-APEEI MRRQ-EDDnp	nsh	531	nsh
Abz-APEEI MDRYQ-EDDnp	nsh	123	nsh
Abz-APEEI MDYQ-EDDnp	nsh	296	nsh
Abz-HPVPV YAFSPQ-EDDnp	5230	6867	192
Abz-QPMAV VQSVPQ-EDDnp	4393	1093	129
Abz-QPMDV VQSVPQ-EDDnp	<1	nsh	17

[a] nsh, non-significant hydrolysis.

TABLE 3
Specificity constants k_{cat}/K_m for the hydrolysis of proteinase 3-directed FRET substrates

Values are means of at least three experiments. The error for k_{cat}/K_m is <15%. Cleavage sites are indicated by a space in the peptide sequence.

	k_{cat}/K_m		
	mPr3	hPr3	mNE
		$m_M^{-1}s^{-1}$	
Abz-VADC ADQ-EDDnp	nsh[a]	614	nsh
Abz-VADC RDRQ-EDDnp	15	6,500	nsh
Abz-VADC ADYQ-EDDnp	18	11,379	nsh
Abz-VARC RDRQ-EDDnp	181	40	nsh
Abz-VARC ADYQ-EDDnp	**1,077**	388	nsh

[a] nsh, non-significant hydrolysis.

[4] The nomenclature used for the individual amino acid residues (*e.g.* P1, P2, etc.) of a substrate and corresponding residues of the enzyme subsites (*e.g.* S1, S2, etc.) is that of Schechter and Berger (32).

both hNE and mNE at the VY bond, bears no charge at these positions as well (Table 2). Of interest, when we compared the electrostatic surface potentials of mNE and hNE, we found that the S side of mNE active site was far more negative than that of hNE (Fig. 3), which may explain why mNE does not accommodate the E–E pair at P2–P3 in hNE substrates (Table 2). On the S′ side, the two L → R amino acid substitutions at position 143 and position 35 in mNE also create a positively charged environment close to S2′ and possibly S3′ subsites (Fig. 3*B*). This may explain why hNE substrates with positively charged residues at P2′ and/or P3′ are not accommodated by mNE. But substitution in hNE substrates of one or the two positively charged residues at P2′ and P3′ by negative or neutral residues did not allow cleavage by mNE (Table 2). Because Abz-HPVPVYAFSPQ-EDDnp is cleaved by all three mouse NSPs, we sought to produce a mNE-specific FRET substrate from a sequence in a natural NE substrate, which has neither charged residues at P2–P3 and P2′–P3′ nor a putative cleavage site for cathepsin G. We identified such a sequence in both mouse and human leukemogenic PML-RARα protein (24). The resulting substrate Abz-QPMAVVQSVPQ-EDDnp was indeed rapidly hydrolyzed by mNE with a k_{cat}/K_m in the 10^6 $M^{-1}s^{-1}$ range (Table 2). Although this peptide was resistant to cleavage by mCG, it was cleaved at the V–V bond 34 times more slowly by mPr3. When we attempted to prevent mPr3-mediated hydrolysis by introducing a negatively charged residue at the P2 position (Abz-QPMDVVQSVPQ-EDDnp), the resulting substrate was no longer cleaved by mNE probably due to the electronegative surroundings of mNE S2–S3 subsites. Our strategy to introduce a single negative charge at P3 failed as well but did confirm that the hNE-APEEIMDRQ-EDDnp substrate was not cleaved by mNE because of its unprimed negative sequence.

Generation of an mPr3 Substrate following Specific Amino Acid Substitution in hPr3 Substrates—We have previously identified critical residues in the reactive site of human Pr3 that contribute to its substrate specificity. These are Lys^{99} at the S2 subsite, Asp^{61} at both S1′ and S3′, and most importantly Arg^{143} at the S2′ subsite (21). Interestingly, Asp^{61} and Arg^{143} remained conserved while Lys^{99} was substituted with Asn^{99} in mPr3 (25) (Fig. 4*A*). Features of hPr3 substrates are characterized by a negatively charged residue at P2 that is accommodated within the S2 lysyl-containing subsite (Table 3). We replaced the P2 aspartyl residue by an arginyl residue in the lead human Pr3 sub-

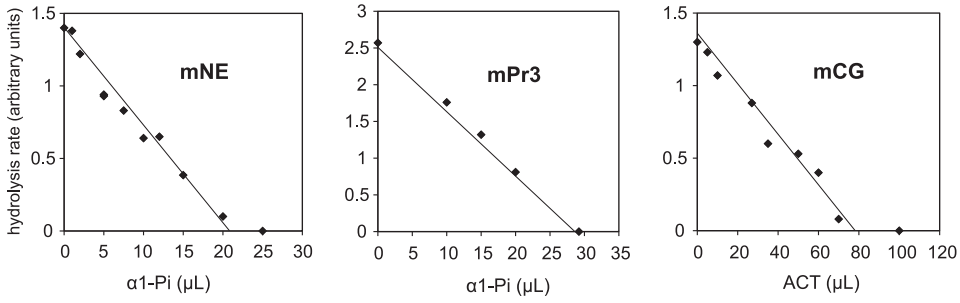

FIGURE 2. **Titration of purified active mNE and mPr3 against human serpin α1-P_i and mCG against human ACT.** Purified proteases were incubated with increasing amounts of titrated inhibitors for 15 min before starting the reaction with appropriate FRET substrates. Fluorescence was recorded spectrofluorometrically for 3–5 min. Purified protease working solutions were all in the nanomolar range. Working solutions of inhibitors were 6 nM, 15 nM, and 3.6 nM for mNE, mPr3, and mCG, respectively, in accordance with the protease concentrations.

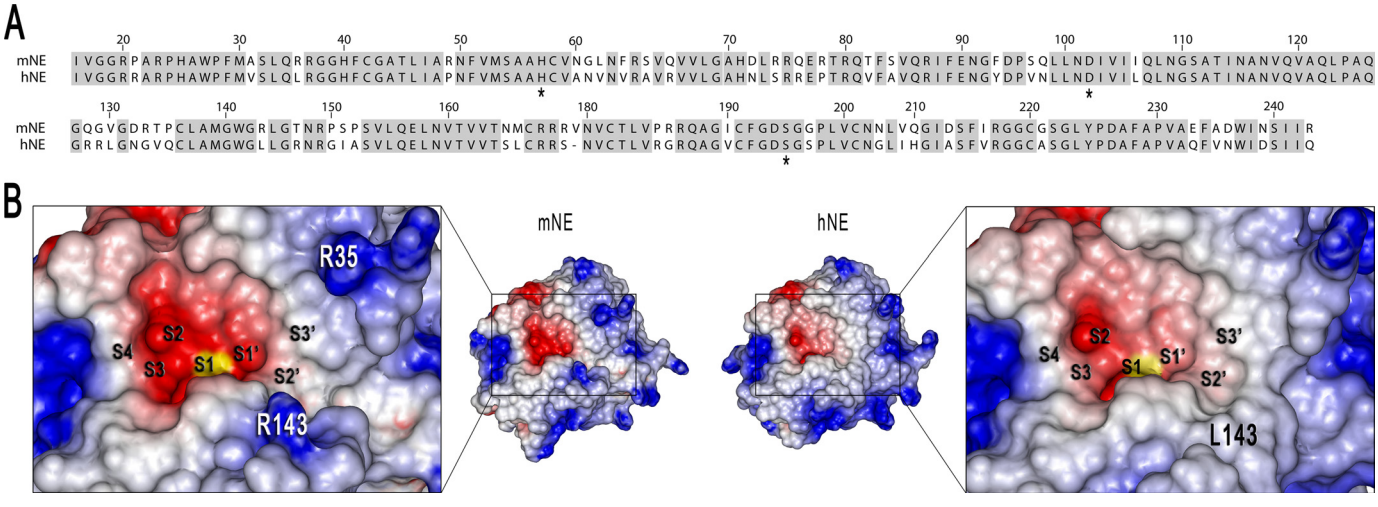

FIGURE 3. **Active site region of murine elastase compared with that of human elastase.** *A*, the sequence of murine neutrophil elastase (mNE) was aligned with its orthologous human counterpart (hNE) using Jalview. Identical residues are shown against a gray background. Residue numbers based on the chymotrypsinogen sequence numbering system are indicated above the alignment. *Asterisks* denote the position of the amino acids of the catalytic triad (His^{57}, Asp^{102}, and Ser^{195}). Amino acid sequences were from UniProtKB data base files ELNE_MOUSE and ELNE_HUMAN for mouse and human elastase, respectively. *B*, the solvent-accessible surface of each protease is colored to show its positive (*dark blue*) and negative (*red*) electrostatic potential calculated with DELPHI software. The *boxed region* of each protease, which corresponds to the active site region, has been enlarged to show the location of S4 to S3′ subsites as inferred from the side-chain location of the P4–P3′ residues of OMTKYIII inhibitor complexed to HNE (PDB accession number: 1PPF). In the *close-up view*, the catalytically active serine (Ser^{195}) is colored *yellow*. Charged critical residues that lie in the vicinity of the active site are indicated. The main difference lies in residues lining the S2′ subsite of both proteases where the neutral Leu^{143} in hNE is replaced by a positively charged arginyl residue (Arg^{143}) in mNE. The substitution of Leu for Arg at position 35 in mNE may also have an influence on the P3′ specificity. The contour lines of electrostatic potential are −5 *kT/e* (*red*) and +5 *kT/e* (*blue*). Model of murine elastase was built as described under "Experimental Procedures," and the atomic coordinates for human NE were extracted from PDB file 1PPF.

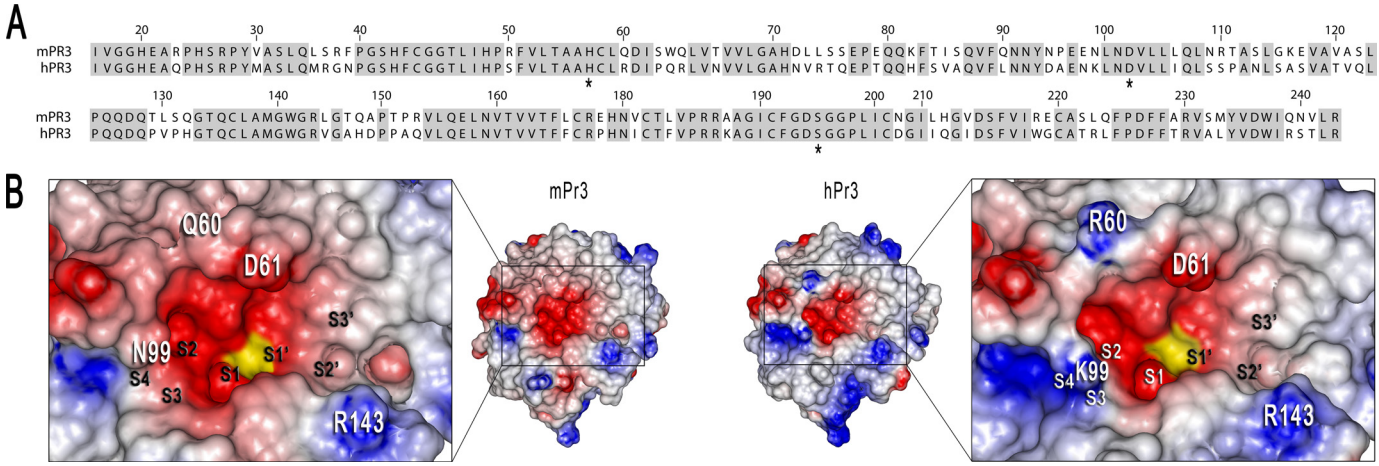

FIGURE 4. **Comparison of murine and human proteinase 3 active sites.** *A*, alignment of murine (UniProtKB accession name PRTN3_MOUSE) and human (UniProtKB accession name PRTN3_HUMAN) proteinase 3 sequences showing identical (*gray background*) and substituted residues between both sequences. Amino acid numbers correspond to those of the chymotrypsinogen sequence. *Asterisks* denote the position of the amino acids of the catalytic triad (His[57], Asp[102], and Ser[195]). *B*, values of electrostatic potentials (calculated as in Fig. 3) of murine and human proteinase 3 were mapped onto the solvent-accessible surface of each protease. Positive and negative regions of the molecular surface are colored *blue* and *red*, respectively. Critical charged residues suspected in substrate specificity are indicated in the *close-up view* of the protease active site (*boxed region*). Note the positive residues Arg[60] and Lys[99] of the substrate binding region in hPr3 are replaced by the neutral Gln[60] and Asn[99] in mPr3, respectively. The structural model of mPr3 was derived from hPr3 x-ray structure (PDF file: 1FUJ) by homology modeling as described under "Experimental Procedures." Positioning of the S4 to S3′ subsites was assessed as in Fig. 3. The catalytic serine (Ser[195]) is colored *yellow*.

strate, Abz-VA(D→R)CRDRQ-EDDnp. Hydrolysis of the new substrate, Abz-VARCRDRQ-EDDnp, resulted in a 12-fold increase of mPr3 k_{cat}/K_m while hPr3 k_{cat}/K_m decreased by 160-fold (Table 3). Its cleavage site, C–R bond, remained unchanged as judged by comparison of the reversed-phase HPLC retention time of the EDDnp-containing peptide with that of hPr3-cleaved Abz-VADCRDRQ-EDDnp (21). Of note, neither mNE nor mCG cleaved Abz-VARCRDRQ-EDDnp. To improve the sensitivity of this substrate to mPr3 we substituted the P′ sequence -RDRQ- with the sequence -ADYQ-, which increased cleavage susceptibility of hPr3 substrates (21) (Table 3). The k_{cat}/K_m values for both mPr3 and hPr3 increased significantly suggesting that the S′ subsites are less important for discriminating between hPr3 and mPr3. Mouse Pr3 did not cleave the hPr3 substrate derived from the NFκB internal sequence that also contains an aspartyl residue at P2 (21) further highlighting the importance of the S2 subsite for discriminating between human and mouse Pr3. In support of these observations, analysis of the three-dimensional model of mPr3 confirmed that the main difference between the mouse and human Pr3 resides in the S2 subsite (Fig. 4*B*); the R60Q and K99N substitutions generated an overall negative environment surrounding the S2 subsite in mPr3. This is also reflected by the fact that mouse Pr3 had a more negative net charge than human Pr3 (Table 1). Unlike their S subsites, the overall conformations of the S′ subsites of the mouse and human Pr3 seem to be very similar (Fig. 4*B*).

Targeted Changes in hCG Amino Acid Substrates Explain mCG Substrate Specificity—Contrary to mNE and mPr3, mCG cleaved hCG substrates particularly the FRET peptide Abz-TPFSGQ-EDDnp with a far better k_{cat}/K_m value (Table 4). This latter peptide is derived from hCG protein substrate, the protease-activated thrombin receptor PAR-1 (26). Of interest, hCG-mediated cleavage at the F–S bond was conserved in mCG. The other sensitive hCG peptide, Abz-EPFWEDQ-EDDnp, a peptide derived from the reactive loop of the human serpin ACT, was also cleaved by mCG at the F–W bond (Table 4). Of note, human ACT inhibits not only hCG but also mCG.

TABLE 4

Specificity constants k_{cat}/K_m for the hydrolysis of cathepsin G-directed FRET substrates

Values are means of at least three experiments. The error for k_{cat}/K_m is <15%. Cleavage sites are indicated by a space in the peptide sequence.

	k_{cat}/K_m			
	mCG	hCG	mNE	mPr3
	$mM^{-1}s^{-1}$			
Abz-TPF SGQ-EDDnp	5500	162	nsh[a]	nsh
Abz-EPF WEDQ-EDDnp	543	243	nsh	nsh

[a] nsh, non-significant hydrolysis.

To better our understanding of mCG-FRET peptide substrate interaction, molecular modeling studies revealed that only slight differences in the partition of charged residues between mCG and hCG reside in the surrounding of active site (Fig. 5*B*) indicating that mCG and hCG might exhibit similar substrate specificity. There remains, however, some obvious difference namely the hCG Arg at position 41 in the vicinity of the S2′ binding sites that is replaced with Ala in mCG (Fig. 5*B*). Such difference does not prevent mCG and hCG from accommodating a negatively charged residue at P2′ as observed using the Abz-EPFWEDQ-EDDnp substrate. However, if a positive residue was present at P2′, it could possibly impair interaction with hCG, but not (or to a lesser degree) mCG. To test this hypothesis, we replaced the P2′ D residue in the polyvalent MNEI-derived Abz-GIATFCDLMPEQ-EDDnp substrate cleaved at the F–C bond by hCG, by an Arg residue. Analysis of substrate cleavage found that the Arg-containing substrate was cleaved 10 times more slowly by hCG, and ~3 times faster by mCG suggesting that the S2′ subsite in cathepsin G is important for substrate binding and that residue at position 41 is involved in the P2′ specificity of cathepsin G (Table 5). Another

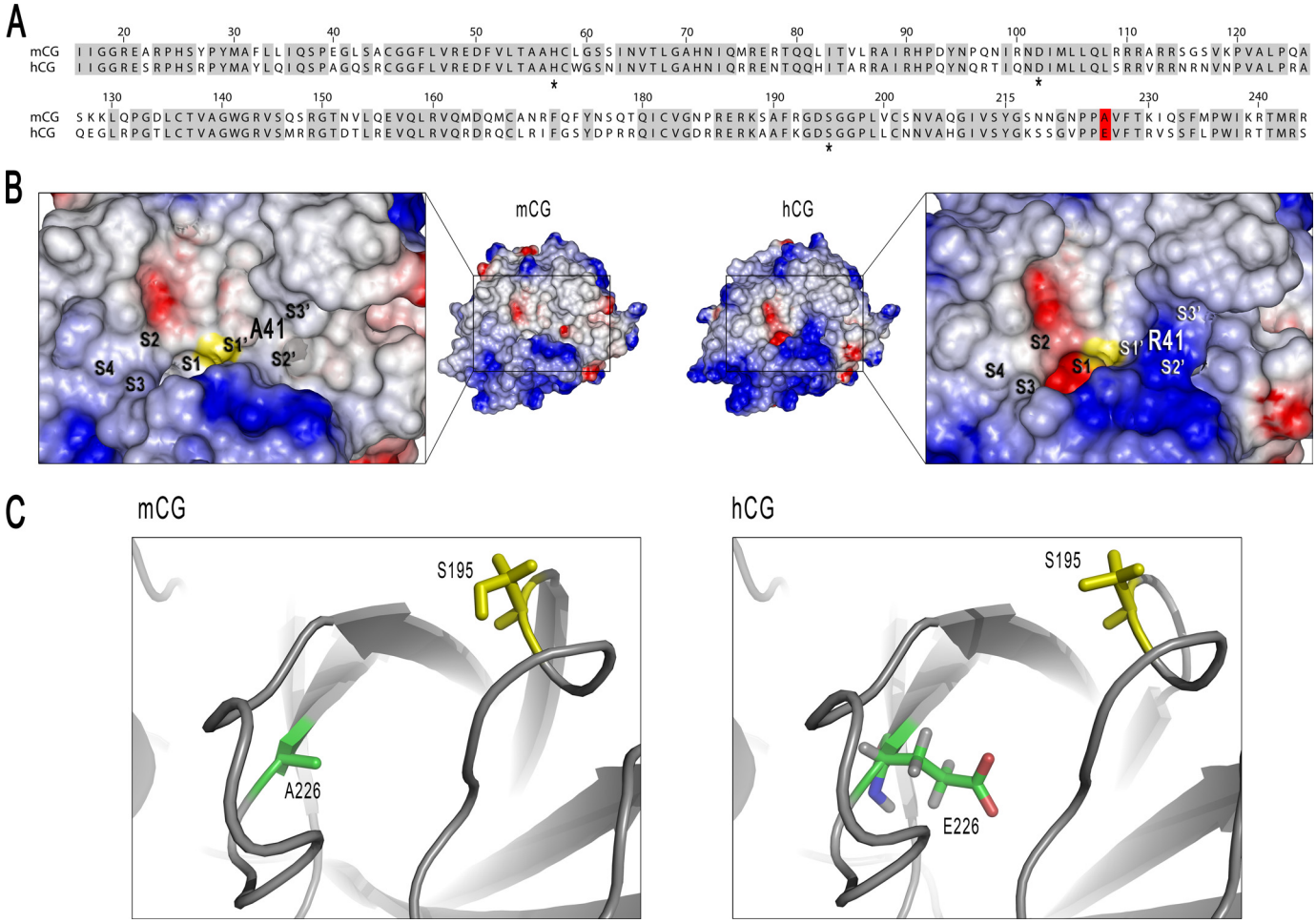

FIGURE 5. **Compared structures of the active site regions of murine and human cathepsin G.** *A*, sequence alignment for murine (UniProtKB accession name CATG_MOUSE) and human (UniProtKB accession name CATG_HUMAN) cathepsin G. *Asterisks* denote the position of the amino acids of the catalytic triad (His[57], Asp[102], and Ser[195]). The critical Glu[226] (chymotrypsinogen numbering) of the S1 pocket of hCG is replaced by an alanyl residue in mCG. Both residues are shown against a *red background*. *B*, the solvent-accessible surface of mCG and hCG has been colored according to values of electrostatic potentials calculated with DELPHI software (*blue*, positive; *red*, negative; *yellow*, catalytic Ser[195]). The positively charged Arg[41] in hCG active site is substituted by the neutral and small Ala residue in mCG. As seen in the zoomed view of each active site (*boxed region*), this leads to major differences in the shape and charge of the S2′–S3′ binding region. mCG model was built by comparative modeling techniques (see "Experimental Procedures") based on the hCG x-ray structure (PDB accession number 1CGH). Location of S4 to S3′ subsites in each protease active site was inferred as described in Fig. 3. *C*, *close-up view* of the active sites (ribbon representation) of murine CG and human CG. Glu[226] in hCG, which allows accommodation of a Lys side chain in the S1 pocket of hCG, is replaced by an Ala residue in mCG. Both views were prepared with PyMOL (DeLano, W. L. (2002), DeLano Scientific LLC, San Carlos, CA).

TABLE 5

P2′ specificities of mouse and human cathepsin Gs

Values are means of at least three experiments. Cleavage sites are indicated by a space in the peptide sequence.

	Fluorescence	
	mCG	hCG
	arbitrary units	
Abz-GIATF CDLMPEQ-EDDnp	29	600
Abz-GIATF CRLMPEQ-EDDnp	92	51
Abz-TPF SALQ-EDDnp	215	700
Abz-TPK SALQ-EDDnp	<2	70

difference between hCG and mCG G is the absence of Glu[226] at the bottom of the S1 pocket in mCG (Fig. 5*C*). This negatively charged residue could explain why both P1-Phe and P1-Lys residues are accommodated in the hCG S1 pocket (27). Consequently, unlike its human homolog, mCG should not cleave after Lys residues. This assumption was tested by comparing cleavage rates of two FRET substrates that differed only by Phe or Lys at P1, by hCG and mCG. Under similar experimental conditions, mCG cleaved only Abz-TPFSALQ-EDDnp at a significant rate, whereas hCG hydrolyzed both Abz-TPFSALQ-EDDnp and Abz-TPKSALQ-EDDnp, although the latter peptide was cleaved ~10 times slower (Table 5).

Potential in Vivo Implications of Our Findings—It is widely accepted that NSPs play a critical role in neutrophil-associated lung inflammatory and tissue-destructive diseases. To investigate NSP pathogenic role(s), various mouse experimental models have been developed that mimic acutely or chronically injured human lungs. As alluded to earlier, the relative contribution of NSPs to lung disease processes as well as their underlying mechanisms remain still poorly understood. And the lack of purified mouse NSPs and their specific substrates have hampered advances in these studies. In this work, we provided evidence that peptide substrate specificities of human and mouse NSPs could be different despite their conserved cleft and close structural resemblance. We then went on to identify key residues in the vicinity of the active sites of human and mouse

NSPs, which account for these specificities. It must be emphasized that the positioning of charged residues contributes, but may not fully explain, the observed substrate specificity in both types of proteases.

In any event, mouse and human NSPs may well generate different peptide profiles from a common substrate. For example, hNE and mNE generate chemotactic elastin peptides that differ structurally (but not functionally) (28). Because of its different S2 specificity mPr3 does not cleave the hPr3 substrate deduced from the internal sequence of NFκB whose cleavage impacts cytokine network and cell viability during inflammation (29). Because mouse NFκB has the same internal sequence as its human counterpart, this raises the question of the role of mPr3 as a NFκB-degrading protease that influences the endothelial cell response during inflammation. We also showed that mCG does not cleave after Lys residues, unlike hCG, because it appear to lack a negatively charged residue at the bottom of the S1 pocket. In addition, hCG poorly accommodates positively charged residues in its S2′ site, while mCG does not. This might significantly influence the physiological function of the mouse protease, which may involve the cleavage of protein substrates. Also, enzyme inhibitors may exhibit different affinities toward mouse and human NSPs. In support of this, eglin C inhibits mPr3 but not hPr3 and recombinant hNE inhibitor Val^{15} aprotinin is a poor inhibitor of mNE (30). Another example is the recently engineered hNE inhibitor, EPI-hNE4. This molecule initially designed as a putative therapeutic for lung inflammatory diseases does not inhibit mNE (23, 31). It must be emphasized that crystal/x-ray structures of mouse neutrophil serine proteases need to be determined to ascertain our findings and gain in-depth insights on the structural differences with their human counterparts. In any event and in light of our findings, data generated from mouse models studying disease pathogenesis or testing NSP inhibitors should be cautiously interpreted before extrapolation to human situations. Also, inhibition strategies of human NSPs using mice as experimental models (intermediate step) should take into consideration the differences in substrate specificities between mouse and human NSPs.

In conclusion, the availability of mice deficient in NSPs should continue to help define the relative contribution of these proteases in neutrophil-associated lung diseases. The identified structural differences between human and mouse NSPs and the now available peptide substrates to specifically detect/quantify either mNE, mCG, and/or mPr3 should better our understanding of NSP roles in disease pathogenesis.

Acknowledgment—We thank Valérie Labas, Institut National de la Recherche Agronomique, Tours-Nouzilly for performing mass spectrometry analyses.

REFERENCES

1. Bode, W., Meyer, E., Jr., and Powers, J. C. (1989) *Biochemistry* **28,** 1951–1963
2. Ganz, T. (1999) *Proc. Assoc. Am. Physicians* **111,** 390–395
3. Belaaouaj, A. (2002) *Microbes Infect.* **4,** 1259–1264
4. Lee, W. L., and Downey, G. P. (2001) *Am. J. Respir. Crit. Care Med.* **164,** 896–904
5. Birrer, P. (1995) *Respiration* **62,** Suppl. 1, 25–28
6. Janoff, A. (1985) *Am. Rev. Respir. Dis.* **132,** 417–433
7. Kawabata, K., Hagio, T., and Matsuoka, S. (2002) *Eur. J. Pharmacol.* **451,** 1–10
8. Mahadeva, R., and Shapiro, S. D. (2002) *Thorax* **57,** 908–914
9. Wright, J. L., Cosio, M., and Churg, A. (2008) *Am. J. Physiol. Lung Cell Mol. Physiol.* **295,** L1–L15
10. Eriksson, S. (1965) *Acta Med. Scand. Suppl.* **432,** 1–85
11. Sandford, A. J., Weir, T. D., and Paré, P. D. (1997) *Eur. Respir. J.* **10,** 1380–1391
12. Lafuma, C., Frisdal, E., Harf, A., Robert, L., and Hornebeck, W. (1991) *Eur. Respir. J.* **4,** 1004–1009
13. Belaaouaj, A., Moog-Lutz, C., Just, J., Houzel-Charavel, A., Shapiro, S. D., and Cayre, Y. (1999) *Mamm. Genome* **10,** 210–212
14. Belaaouaj, A., Walsh, B. C., Jenkins, N. A., Copeland, N. G., and Shapiro, S. D. (1997) *Mamm. Genome* **8,** 5–8
15. Hohn, P. A., Popescu, N. C., Hanson, R. D., Salvesen, G., and Ley, T. J. (1989) *J. Biol. Chem.* **264,** 13412–13419
16. Hirche, T. O., Atkinson, J. J., Bahr, S., and Belaaouaj, A. (2004) *Am. J. Respir. Cell Mol. Biol.* **30,** 576–584
17. Kessenbrock, K., Fröhlich, L., Sixt, M., Lämmermann, T., Pfister, H., Bateman, A., Belaaouaj, A., Ring, J., Ollert, M., Fässler, R., and Jenne, D. E. (2008) *J. Clin. Invest.* **118,** 2438–2447
18. Korkmaz, B., Attucci, S., Juliano, M. A., Kalupov, T., Jourdan, M. L., Juliano, L., and Gauthier, F. (2008) *Nat. Protoc.* **3,** 991–1000
19. Serveau, C., Moreau, T., Zhou, G. X., ElMoujahed, A., Chao, J., and Gauthier, F. (1992) *FEBS Lett.* **309,** 405–408
20. Réhault, S., Brillard-Bourdet, M., Juliano, M. A., Juliano, L., Gauthier, F., and Moreau, T. (1999) *J. Biol. Chem.* **274,** 13810–13817
21. Korkmaz, B., Hajjar, E., Kalupov, T., Reuter, N., Brillard-Bourdet, M., Moreau, T., Juliano, L., and Gauthier, F. (2007) *J. Biol. Chem.* **282,** 1989–1997
22. Andersson, K. B., Sletten, K., Berntzen, H. B., Fagerhol, M. K., Dale, I., Brandtzaeg, P., and Jellum, E. (1988) *Nature* **332,** 688
23. Attucci, S., Gauthier, A., Korkmaz, B., Délepine, P., Martino, M. F., Saudubray, F., Diot, P., and Gauthier, F. (2006) *J. Pharmacol. Exp. Ther.* **318,** 803–809
24. Lane, A. A., and Ley, T. J. (2003) *Cell* **115,** 305–318
25. Hajjar, E., Korkmaz, B., and Reuter, N. (2007) *FEBS Lett.* **581,** 5685–5690
26. Attucci, S., Korkmaz, B., Juliano, L., Hazouard, E., Girardin, C., Brillard-Bourdet, M., Réhault, S., Anthonioz, P., and Gauthier, F. (2002) *Biochem. J.* **366,** 965–970
27. Hof, P., Mayr, I., Huber, R., Korzus, E., Potempa, J., Travis, J., Powers, J. C., and Bode, W. (1996) *EMBO J.* **15,** 5481–5491
28. Houghton, A. M., Quintero, P. A., Perkins, D. L., Kobayashi, D. K., Kelley, D. G., Marconcini, L. A., Mecham, R. P., Senior, R. M., and Shapiro, S. D. (2006) *J. Clin. Invest.* **116,** 753–759
29. Preston, G. A., Zarella, C. S., Pendergraft, W. F., 3rd, Rudolph, E. H., Yang, J. J., Sekura, S. B., Jennette, J. C., and Falk, R. J. (2002) *J. Am. Soc. Nephrol.* **13,** 2840–2849
30. Wiesner, O., Litwiller, R. D., Hummel, A. M., Viss, M. A., McDonald, C. J., Jenne, D. E., Fass, D. N., and Specks, U. (2005) *FEBS Lett.* **579,** 5305–5312
31. Delacourt, C., Hérigault, S., Delclaux, C., Poncin, A., Levame, M., Harf, A., Saudubray, F., and Lafuma, C. (2002) *Am. J. Respir. Cell Mol. Biol.* **26,** 290–297
32. Schechter, I., and Berger, A. (1967) *Biochem. Biophys. Res. Commun.* **27,** 157–162